Eur. Phys. J. B **8**, 99–112 (1999)

THE EUROPEAN PHYSICAL JOURNAL B

EDP Sciences

Morphological characterization of spinodal decomposition kinetics

V. Sofonea[1,2] and K.R. Mecke[1,a]

[1] Fachbereich Physik, Bergische Universität Wuppertal, 42097 Wuppertal, Germany
[2] Center for Fundamental and Advanced Technical Research, Romanian Academy, Mihai Viteazul 24, 1900 Timişoara, Romania

Received 3 March 1998

Abstract. The time evolution of the morphology of homogeneous phases during spinodal decomposition is described using a family of morphological measures known as Minkowski functionals. They provide the characteristic length scale L of patterns in a convenient, statistically robust, and computationally inexpensive way. They also allow one to study the scaling behavior of the content, shape, and connectivity of spatial structures and to define the crossover from the early stage decomposition to the late stage domain growth. We observe the scaling behavior $L \sim t^{\alpha}$ with $\alpha = 2/3$, $\alpha = 1/2$, and $\alpha = 1/3$ depending on the viscosity of the fluid. When approaching the spinodal density ρ_{sp}, we recover the prediction $L \sim (\rho - \rho_{sp})^{-1/2}$ for the early time spinodal decomposition.

PACS. 05.70.Fh Phase transitions: general aspects – 64.60.-i General studies of phase transitions – 47.20.Hw Morphological instability; phase changes

1 Introduction

A large variety of complex spatial structures emerge nowadays in many systems considered in statistical physics. We are interested in the complex spatial distribution as well as the dynamics of the structures. A basic problem is how to reduce the spatial information to a finite number of relevant parameters in order to find dynamical equations or to compare experiments and theories. For instance, spatial domains of homogeneous phases evolving during spinodal decomposition exhibit an enormous amount of information in their patterns, which is normally reduced to a single time-dependent scaling length $L(t)$.

Phase separation kinetics is probably the most convenient way to generate irregular spatial patterns on a mesoscopic scale. Such patterns arise after a sudden quench of the homogeneous fluid phase from an initial point situated above the critical temperature, into the two-phase coexistence region where the fluid separates into the coexisting liquid and vapor phases. This happens because the homogeneous phase becomes unstable inside the spinodal domain where density fluctuations are growing instantaneously, yielding an inhomogeneous distribution of vapor phase in liquid and vice versa.

In the case of phase separation kinetics one can distinguish two different time regimes [1,2]: the early stage of spinodal decomposition and the late stage of domain growth. During the spinodal decomposition regime, unstable density fluctuations grow and form finally homogeneous domains well separated by an interface. The typical size of these homogeneous domains of coexisting phases increases in the late stage driven by various mechanisms.

The usual approaches to the characterization of the evolution of the single-phase domains which arise after the quenching are mainly based on the time dependent mean domain size $R(t)$ which may be calculated from the first zero of the radial distribution function, or from the first moment of the structure factor [3,4]. Besides being computationally expensive, the mean domain size alone cannot account for the rich variety of geometrical shapes of single phase domains which arise after the quenching, as well as their connectivity. Therefore, it is useful to look for a quantitative characterization of the morphology of spatial patterns which allows one to gain relevant information on the kinetics of many particle systems, especially when these systems undergo phase transitions such as spinodal decomposition [5].

In particular, we address the question whether the morphology of the patterns scale with a characteristic length. As mentioned, the usual method to describe the spatial structure of the system is the density correlation function from which one can extract a typical length scale. But, the correlation function does not give information about the morphology of the structure. In contrast, the morphological measures supplied by integral geometry, known as *Minkowski functionals*, which are introduced in Section 3 of this paper provide means to define the characteristic length scale, as well as a possibility to consider the time evolution of the morphology in a convenient and fast way. In particular, it is possible to define the crossover

[a] e-mail: mecke@wptsb.physik.uni-wuppertal.de

from the early stage decomposition to the late stage domain growth on the basis of significant changes which arise during the time dependence of the morphological measures.

The Minkowski functionals are well known in digital picture analysis [6,7] and integral geometry [8] when dealing with the morphology of black and white discretized images. In two dimensions, these functionals are related to familiar geometric quantities: the area, the boundary length and the connectivity of the spatial pattern. The aim of this paper is to make an attempt towards the characterization of the time evolution of the morphology of phase separation, using these measures.

The paper is organised as follows. In Section 2 we give (for completeness) a brief outline on the 2D hexagonal lattice Boltzmann model [9–11] which was used for subsequent simulations. In Section 3 the Minkowski functionals are introduced paying attention to the way their values are computed on the 2D hexagonal lattice. Section 4 deals with the typical time evolution of the Minkowski functionals during the spinodal decomposition, while in Section 5 two major problems are investigated: (a) the behavior of the characteristic length L of the spinodal decomposition when the mean fluid density approaches the spinodal line and (b) the existence of different scaling regimes $L \sim t^{\alpha}$ in the late stage of domain growth.

2 Lattice Boltzmann model

Spinodal decomposition kinetics has been the subject of considerable attention in recent years. A particular effort was focused on the identification of different scaling regimes. Several appropriate computer simulation techniques (molecular dynamics [12–14], Langevin models [15, 16], lattice gas [17–19] or lattice Boltzmann models [9–11, 20–22]) for the spinodal decomposition have been developed.

Lattice gas models for simple or complex fluids, developed in the past decade, provide a convenient tool to study hydrodynamics [23], as well as phase separation kinetics [18,24]. These models always start from the microscopic level, where particles move across a discrete lattice and interact themselves via collisions and long-range potentials. At the macroscopic level (*i.e.*, at a spatial scale larger than a lattice unit), lattice gas models are able to simulate hydrodynamic flows, fluid mixtures including interfaces, phase transitions and multiphase flows, as described in the review paper [19] and references therein.

Lattice Boltzmann models [25,27,28], which use particle distribution functions moving on the discrete lattice (instead of integer particle numbers) were subsequently developed in order to reduce the statistical noise inherent to former lattice gas models, while keeping their major advantages, in particular, the amenability to parallel computing. For example, the modeling of the isothermal hydrodynamics of a two phase system was achieved in references [9–11] using a lattice Boltzmann model on a $2D$ hexagonal lattice with unit vectors $\mathbf{e}_i = \{\cos[2\pi(i-1)/6]\ ,\ \sin[2\pi(i-1)/6]\}$. We use this model to simulate time-evolving patterns whose morphological description is the main objective of this paper. We briefly review the method and refer the interested reader to references [9–11] for more information.

The particle distribution functions $f_i(\mathbf{x},t)$ evolve in accordance to the discretized Boltzmann equation

$$f_i(\mathbf{x}+c\mathbf{e}_i, t+1) - f_i(\mathbf{x},t) = \Omega_i(\mathbf{x},t) \tag{2.1}$$

with $c = 1$. The collision term $\Omega_i(\mathbf{x},t)$ is linearized introducing the equilibrium distribution functions f_i^{eq}, $i = 0,1,\ldots 6$, as well as the relaxation time τ

$$\Omega_i = -\frac{1}{\tau}(f_i - f_i^{eq}). \tag{2.2}$$

The relaxation time τ has a lower bound ($\tau > 1/2$), because of the amplification of differences from the equilibrium distribution f_i^{eq} in equation (2.1).

The equilibrium distribution functions $f_i^{eq}(\mathbf{x})$ were expanded as power series in the local velocity $\boldsymbol{u}(\mathbf{x})$

$$\begin{aligned} f_i^{eq} &= A + Be_{i\alpha}u_\alpha + Cu^2 + Du_\alpha u_\beta e_{i\alpha}e_{i\beta} + F_\alpha e_{i\alpha} \\ &\quad + G_{\alpha\beta}e_{i\alpha}e_{i\beta} + \cdots \qquad (i = 1,\ldots,6; \quad \alpha = 1,2) \\ f_0^{eq} &= A_0 + C_0u^2 + \cdots \end{aligned} \tag{2.3}$$

and the appropriate coefficients were determined using local conservation of mass and momentum, as well as Galilean invariance and isotropy of pressure tensor [9]

$$P_{\alpha\beta} = p\,\delta_{\alpha\beta} + \kappa\,\frac{\partial\rho}{\partial x_\alpha}\,\frac{\partial\rho}{\partial x_\beta} \tag{2.4}$$

where

$$p = p_0 - \kappa\rho\nabla^2\rho - \frac{\kappa}{2}|\nabla\rho|^2. \tag{2.5}$$

Here

$$\rho = \rho(\mathbf{x},t) = \sum_{i=0}^{i=6} f_i(\mathbf{x},t) \tag{2.6}$$

is the local particle density, the constant κ defines the strength of the surface tension and $p_0 = \rho\psi'(\rho) - \psi(\rho)$ is the state equation of the fluid.

In order to have a van der Waals fluid, the bulk free energy density ψ has the form

$$\psi = \rho T \ln\left(\frac{\rho}{1-\rho b}\right) - a\rho^2 \tag{2.7}$$

where T is the system temperature. Choosing $a = 9/49$, $b = 2/21$, the critical temperature value becomes $T_c = 0.571$. The spinodal densities $\rho_{sp}^{\pm}$ at temperature $T < T_c$ are defined as the zeroes of the equation $\psi''(\rho) = 0$. For $T = 0.550$, one obtains the densities $\rho_{sp}^{-} = 2.744$ and $\rho_{sp}^{+} = 4.315$. Figure 1 shows the phase coexistence diagram $(T-\rho)$, as well as the spinodal curve $(T-\rho_{sp})$ obtained from the bulk free energy density (Eq. (2.7)) with the values of a and b mentioned above.

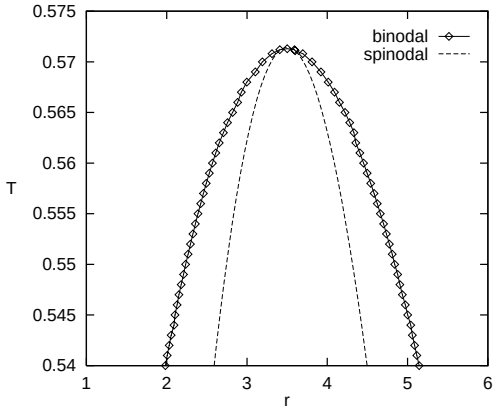

Fig. 1. Phase coexistence diagram (diamonds) and the spinodal curve (dashed line) of the van der Waals fluid given by the bulk free energy density (Eq. (2.7)) ($a = 9/49$, $b = 2/21$).

A particular attention was given to the computing of the spatial derivatives of the local density $\rho(\mathbf{x})$

$$\nabla\rho(\mathbf{x}) \simeq \frac{1}{3}\sum_{i=1}^{i=6}\rho(\mathbf{x}+\mathbf{e}_i)\,\mathbf{e}_i \tag{2.8}$$

$$\nabla^2\rho(\mathbf{x}) \simeq \frac{2}{3}\left[\sum_{i=1}^{i=6}\rho(\mathbf{x}+\mathbf{e}_i) \;-\; 6\,\rho(\mathbf{x})\right]. \tag{2.9}$$

These relations were obtained from the Taylor's expansion of $\rho(\mathbf{x})$, taking into account the sum properties of the lattice vectors $\mathbf{e}_i$ [26].

Simulations were done on lattices with 256×256, 512×512 and 1024×1024 nodes, using periodic boundary conditions. Each simulation run was defined by the value of the mean density ρ, and the value of the relaxation time τ (which gives also the value of the kinematic viscosity $\nu = (2\tau - 1)/8$ [9]). Most simulations were done with the value $\kappa = 0.01$ of the surface tension constant, which ensures the width of the interface region between homogeneous phases to be approximatively 10 lattice units.

Computer runs were done as follows. The lattice system was first initialized with a mean density ρ and 1% random fluctuations of the local density $\rho(\mathbf{x})$ were allowed around the mean value. After each initialisation, the system was released to evolve during 500 preliminary automaton steps at the initial temperature $T_{in} = 0.580$ above the critical one, then the temperature was suddenly changed to the final value $T_{fin} = 0.550$. Starting from this moment ($t = 0$), the system was allowed to evolve to its equilibrium state while snapshots were achieved at certain time intervals. Snapshots were characterized through the corresponding values of the Minkowski functionals defined in the next section.

3 Morphological measures

The morphological characterization of patterns is clearly important to statistical physics, since complex spatial structures emerge nowadays in many physical systems under consideration. The specification of spatial patterns requires *topological* as well as *geometrical* descriptors to characterize not only the connectivity but also the content and shape of figures. The aim of this section is to point out that integral geometry supplies a suitable family of such descriptors, known as *Minkowski functionals*. In a d-dimensional ambient space the number of these functionals is $d + 1$. We are primarily interested in the two-dimensional case, where the Minkowski functionals are related with familiar measures: covered area, boundary length and Euler characteristic. Integral geometry provides not only morphological measures to describe random structures in space but also powerful theorems and formulae which make the calculus convenient for many models of stochastic geometries.

Since the methods of integral geometry are not widely-known among physicists, we compile some pertinent facts [8] in this section. First, we introduce the notion of a morphological measure for an homogeneous domain A as an additive, motion invariant and conditional continuous functional $\mathcal{W}(A)$. In a second step we present a theorem which asserts that each morphological measure is a linear combination of the $d+1$ Minkowski functionals in d dimensions. These functionals are well-known quantities in digital picture analysis [6] and mathematical morphology [7].

3.1 Minkowski functionals

First, we define what we want to call a morphological measure. Let us consider a homogeneous domain $A = \cup_i K_i$ which can be represented as a finite union of compact convex sets K_i (for instance, hexagons in Fig. 2). Let $\mathcal{R}$ denote the class of subsets of $\mathbb{R}^d$ which can be represented as a finite union of compact convex sets K_i, *i.e.*, $A \in \mathcal{R}$ if and only if $A = \cup_{i=1}^{N} K_i$. Morphological measures are defined as functionals $\mathcal{W}\colon \mathcal{R} \to \mathbb{R}$ on homogeneous domains. Nearly every continuous pattern can be decomposed in convex subsets. For instance, due to a finite resolution of the experimental equipment or due to simulations on a lattice one has often an underlying pixel structure. Each pixel (squares or hexagons in two dimensions) is a compact, convex set and the whole pattern is the union of all of these pixels. In Figure 2 we show an example of such a lattice structure.

Let us now define three general properties a functional $\mathcal{W}\colon \mathcal{R} \to \mathbb{R}$ should possess in order to be a morphological measure.

(i) *Additivity.* The functional of the union $A \cup B$ of two domains $A, B \in \mathcal{R}$ equals the sum of the functional of the single domains subtracted by their intersection

$$\mathcal{W}(A \cup B) = \mathcal{W}(A) + \mathcal{W}(B) - \mathcal{W}(A \cap B). \tag{3.1}$$

This relation generalizes the common rule for the addition of the volume ($d = 3$) or area ($d = 2$) of two domains. The measure of the double-counted intersection has to be substracted as for the volume, for

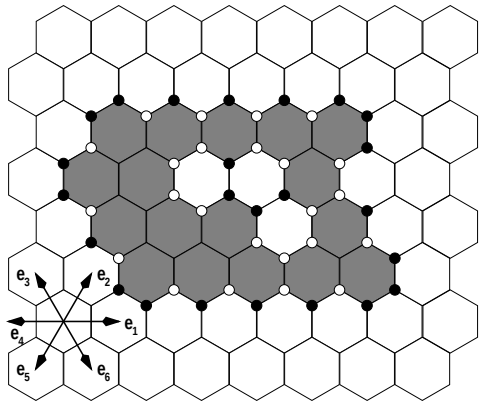

Fig. 2. 2D array of $N = 64$ black and white hexagonal pixels centered on the lattice nodes. Particles can stay at their lattice site or they can move in six directions along the unit vectors $\mathbf{e}_i$ of the lattice. At each lattice site the density $\rho = \sum_{i=0}^{6} f_i$ is given by the sum of the distribution functions f_i denoting the probability to find a particle moving in the direction $\mathbf{e}_i$. "Local curvature" values are assigned to the corners of each black pixel, as follows : corners marked "•" have the value -2, corners marked "○" have the value 1, while non marked corners have the value 0.One can define the boundary length U on the lattice by the number of edges between black and white pixels ($U = 48/N$ for the configuration above). The area F is given by the number of white pixels ($F = 17/N$) and the Euler characteristic χ by the sum of curvature variables ($\chi = 24(-2) + 30(0) + 48(-1) = 0$).

instance. Only if the volume (area) of the intersection is zero, *e.g.*, for two different hexagons in Figure 2, the relation (3.1) reduces to the usual additivity.

(ii) *Motion invariance.* Let $\mathcal{G}$ be the group of motions, *i.e.*, translations and rotations in $\mathbb{R}^d$. The transitive action of $g \in \mathcal{G}$ on a domain $A \in \mathcal{R}$ is denoted by gA. Then the morphological measure is invariant,

$$\mathcal{W}(gA) = \mathcal{W}(A), \tag{3.2}$$

i.e., the morphological measure of a domain A is independent of its location and orientation in space.

(iii) *Continuity.* If a sequence of convex sets K_n converges towards the convex set K for $n \to \infty$, (with convergence $K_n \to K$ defined in terms of the Hausdorff metric for sets), then

$$\mathcal{W}(K_n) \to \mathcal{W}(K). \tag{3.3}$$

Intuitively, this continuity property expresses the fact that an approximation of a convex domain K by convex polyhedra K_n, for example, also yields an approximation of $\mathcal{W}(K)$ by $\mathcal{W}(K_n)$. We emphasize that we require this condition only for the morphological measure of a convex set and not for unions of them.

In three-dimensional space we can immediately find examples of morphological measures which obey the three conditions (i–iii). For instance, the volume V and the surface area S of a domain A are continuous, motion invariant and additive. In two dimensions, the area F and the boundary length U of a domain may be identified as morphological measures in the sense described above.

Naturally, the question arises if there are other measures which obey the conditions (i–iii) and if there is a systematic way to find such measures. In order to answer this question we introduce the Euler characteristic χ as a prominent member of the family of morphological measures.

The Euler characteristic is introduced first for convex sets K by

$$\chi(K) = \begin{cases} 1, & K \neq \emptyset \text{ is convex,} \\ 0, & K = \emptyset. \end{cases} \tag{3.4}$$

and then extended to $\mathcal{R}$ via the additivity relation (Eq. 3.1),

$$\chi(A \cup B) = \chi(A) + \chi(B) - \chi(A \cap B) \tag{3.5}$$

for any $A, B \in \mathcal{R}$. In particular, for the union $\cup_{i=1}^{N} K_i$ of convex domains one finds

$$\begin{aligned} \chi(\cup_{i=1}^{N} K_i) \;=\; & \sum_i \chi(K_i) - \sum_{i<j} \chi(K_i \cap K_j) + \ldots \\ & + (-1)^{N+1} \chi(K_1 \cap K_2 \cap \ldots \cap K_N) \end{aligned} \tag{3.6}$$

which follows from equation (3.5) by induction. The right hand side of equation (3.6) involves only convex sets and may be applied together with equation (3.4) to compute $\chi(A)$ for any $A \in \mathcal{R}$. We also note that χ: $\mathcal{R} \to \mathbb{Z}$ is motion invariant and it can be shown to agree with the Euler characteristic as defined in algebraic topology [8,29]. Since the Euler characteristic is a constant which equals one for convex sets, it is also continuous, as required by the condition (3.3). Therefore, the Euler characteristic is a morphological measure in the sense given by the conditions (3.1–3.3).

A remarkable theorem in integral geometry is the completeness of the morphological measures. The completeness theorem [29] asserts that any additive, motion invariant and conditional continuous functional $\mathcal{W}(A)$ defined on subsets $A \in \mathcal{R}$, (*i.e.*, any morphological measure) is a linear combination of the $d + 1$ Minkowski functionals,

$$\mathcal{W}(A) = \sum_{\nu=0}^{d} c_\nu W_\nu(A), \tag{3.7}$$

with real coefficients c_ν independent of A. Thus, every morphological measure $\mathcal{W}(\mathcal{A})$ defined by the properties (3.1–3.3) can be written in terms of Minkowski functionals $W_\nu(A)$. In other words, the Minkowski functionals are the complete set of morphological measures. In $d = 3$ they are related with familiar measures: covered volume $V = W_0$, surface area $S = 3W_1$, integral mean curvature $H = 3W_2$ and Euler characteristic $\chi = 3W_3/(4\pi)$. In $d = 2$ the Minkowski functionals are the covered area $F = W_0$, the boundary length $U = 2W_1$, and the Euler characteristic $\chi = W_2/\pi$.

An important consequence of the theorem (3.7) is the possibility to calculate analytically certain integrals

of Minkowski functionals [30]. The "principal kinematical formulae", for instance, describe the factorization of the Minkowski functionals of the intersection $A \cap B$ of two shapes A and B if one integrates over the motions, *i.e.*, the translations and rotations of one of them. A special case of the kinematical formulae is Steiner's formula

$$V_\epsilon(K) = \sum_{\nu=0}^{d} \binom{d}{\nu} W_\nu(K)\epsilon^\nu, \tag{3.8}$$

for the parallel volume V_ϵ of a convex set K, *i.e.*, for the volume of the set of all points within a distance ϵ from the domain K (dilatation). In particular, for $d = 2$ the change

$$\delta F \;\sim\; U\epsilon + \mathcal{O}(\epsilon^2) \tag{3.9}$$

in the covered area F due to an increase of the domain is proportional to the boundary length U. The change in the boundary length itself is proportional to the Euler characteristic.

We emphasize that the Minkowski functional W_ν is homogeneous of order $d-\nu$, *i.e.*, for a dilated domain λA one obtains

$$W_\nu(\lambda A) = \lambda^{d-\nu} W_\nu(A). \tag{3.10}$$

This relation enables one to extract a time-dependent scaling length from the morphological measures in Section 5.

Because of the properties (3.1–3.3) we expect the Minkowski functionals to be suitable measures to characterize the morphology of spinodal decomposition kinetics. These morphological measures have already been applied successfully to the description of microemulsions [30,31], large scale distribution of galaxies in the Universe [32] percolation in porous media [33] and patterns arising in reaction-diffusion systems [34].

Before we apply the Minkowski functionals to describe the morphology of spinodal decomposition kinetics in Section 4, we have to introduce the way these functionals are computed in the case of 2D digital pictures, *i.e.*, 2D arrays whose elements are the local gray level $\rho(\mathbf{x})$ ($0 \le \rho(\mathbf{x}) \le \rho_{max}$), associated with each image point (pixel).

3.2 Thresholding

In order to get detailed information about the spatial structure of spinodal decomposition we want to look at the picture at each density level, *i.e.*, we consider the so-called level contours. Thus, we introduce a threshold density $0 \le \rho_{th} \le \rho_{max}$ and reset the gray value at each pixel to either white or black depending on whether the original value is larger or lower than ρ_{th}, respectively. Here, white corresponds to high values of the gray-level. The qualitative features of the images change drastically when the threshold parameter ρ_{th} is modified. For high thresholds we study the regions of maximum concentration, *i.e.*, we obtain information how the peaks of the profile look like. For low thresholds we study the deep valleys of the concentration profile and for intermediate ρ_{th} we obtain more or less the same visual impression as from the gray-scale pattern. Thus the spatial information we get depends strongly on the threshold we set.

Given a threshold value ρ_{th}, the two-valued (black and white) field $\mathcal{P}(\mathbf{x}, \rho_{th})$ is defined in accordance with

$$\mathcal{P}(\mathbf{x}, \rho_{th}) = \begin{cases} 0, & \rho(\mathbf{x}) < \rho_{th} \\ 1, & \rho(\mathbf{x}) \ge \rho_{th}. \end{cases} \tag{3.11}$$

The null value of $\mathcal{P}(\mathbf{x}, \rho_{th})$ is conventionally associated with a black pixel, while the other value is associated with a white one. In this way, a set of black and white images (corresponding to the different values of the threshold ρ_{th}) may be derived from a single gray-level image and each of these images is characterized by the corresponding field $\mathcal{P}(\mathbf{x}, \rho_{th})$.

3.3 Digital patterns

An array of quadratic pixels is quite often the underlying spatial structure for simulations as well as for experimental data obtained from digital recording equipments [34]. In the case of the 2D hexagonal lattice used for Boltzmann simulations, it would be more convenient to use this lattice structure to calculate directly the Minkowski functionals. In this case, the pixels may be imagined as hexagonal plates, centered on the lattice nodes (Fig. 2) and the gray level may be associated with the local density $\rho(\mathbf{x})$ in each corresponding node. Since the distribution functions $f_i(\mathbf{x}), \quad i = 0, \ldots 6$ in the lattice Boltzmann model are normalized to unity, we have $0 \le \rho(\mathbf{x})$, $\rho_{th} \le \rho_{max} = 7$.

One obvious quantity describing the morphological differences in the images $\mathcal{P}(\mathbf{x}, \rho_{th})$ is the relative white area, $F(\rho_{th})$ *i.e.*, the number $N_{\rho_{th}}$ of the pixels in the original image having the corresponding gray level $\rho(\mathbf{x})$ greater than ρ_{th}, normalized by the total number N of pixels

$$F(\rho_{th}) = \frac{N_{\rho_{th}}}{N} = \frac{1}{N} \sum_{\mathbf{x}} \mathcal{P}(\mathbf{x}, \rho_{th}). \tag{3.12}$$

This quantity decreases from 1 to 0 when the threshold value ρ_{th} is increased from 0 to the maximum value ρ_{max}.

Another morphological quantity is $U(\rho_{th})$, defined as the ratio between the total length $B_{\rho_{th}}$ of the boundary lines separating black and white regions, normalized by the total number of pixels. To determine $B_{\rho_{th}}$, one has to count the numbers of pairs of neighbored black and white pixels, *i.e.*, for the 2D hexagonal lattice

$$\begin{aligned} U(\rho_{th}) &= \frac{B_{\rho_{th}}}{N} \\ &= \frac{1}{N} \sum_{\mathcal{P}(\mathbf{x},\rho_{th})=0} \sum_{i=1}^{i=6} \mathcal{P}(\mathbf{x} + \mathbf{e}_i, \rho_{th}). \end{aligned} \tag{3.13}$$

This quantity always vanishes when ρ_{th} equals its bounding values (*i.e.*, 0 and 7 in the case of our lattice). We note that the boundary length $B_{\rho_{th}}$ does not converge to

the continuous boundary length for a vanishing lattice spacing.

The third quantity of interest, the Euler characteristics $\chi(\rho_{th})$, is defined in two dimensions as the difference between the number of black ($N^b_{\rho_{th}}$) and white ($N^w_{\rho_{th}}$) finite single domains

$$\chi(\rho_{th}) = N^b_{\rho_{th}} - N^w_{\rho_{th}}. \tag{3.14}$$

We do not normalize the Euler characteristic by the total number of pixels in order to keep integer numbers. This quantity describes the connectivity of the domains in the lattice and, *e.g.*, it equals -1 when one has a black drop in a large white lattice and $+1$ *vice versa*.

Despite its global meaning, the Euler characteristics may be calculated in a local way, as already suggested in the case of a square lattice [34]. Figure 2 shows some hexagonal black and white plates covering the nodes of the 2D hexagonal lattice. We assign to each corner of a black pixel the values -2, 1 or 0 depending on the "local curvature". According to Figure 2, the local curvature value is -2 if both of the two nearest neighbors joining at the corner are white, it is 1 if the two nearest neighbors joining there are different, and it is 0 when both nearest neighbors are black. Then the value of the Euler characteristics is given by ($\mathbf{e}_7 \equiv \mathbf{e}_1$)

$$\begin{aligned}\chi(\rho_{th}) = & \\ & \frac{1}{12} \sum_{\mathcal{P}(\mathbf{x},\rho_{th})=0} \sum_{i=1}^{i=6} \Big[-2\,\mathcal{P}(\mathbf{x}+\mathbf{e}_i,\rho_{th})\mathcal{P}(\mathbf{x}+\mathbf{e}_{i+1},\rho_{th}) \\ & + \mathcal{P}(\mathbf{x}+\mathbf{e}_i,\rho_{th})\,[\,1 - \mathcal{P}(\mathbf{x}+\mathbf{e}_{i+1},\rho_{th})\,] \\ & + [\,1 - \mathcal{P}(\mathbf{x}+\mathbf{e}_i,\rho_{th})\,]\,\mathcal{P}(\mathbf{x}+\boldsymbol{e}_{i+1},\rho_{th}) \Big]. \end{aligned} \tag{3.15}$$

One can easy verify that equation (3.15) gives 0 for the case shown in Figure 2 and $+1$ for a single white drop independently of its shape.

It can be shown that this definition of χ possesses a continuum limit for smooth boundaries, which is equal to the integral of the curvature along the boundary lines [8,29]. Thus, $\chi/(UN)$ describes the mean curvature of the boundary line separating black and white domains.

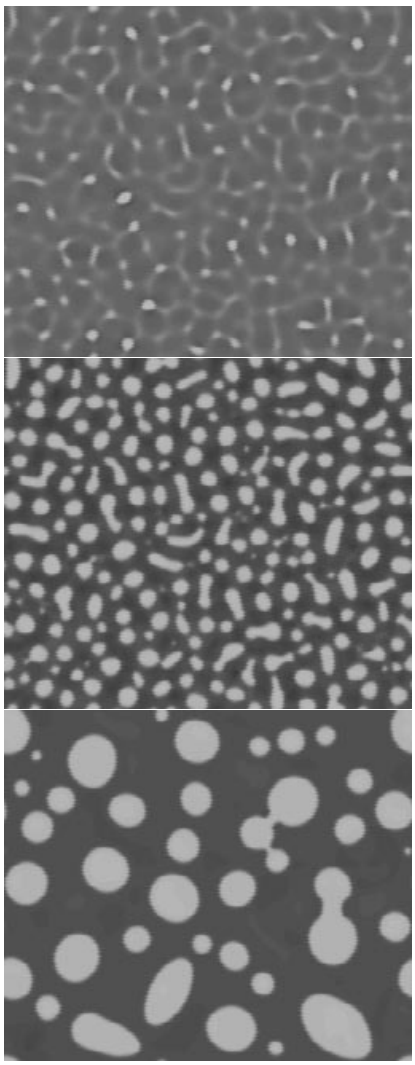

Fig. 3. Time evolution of the local density $\rho(\mathbf{x})$ across a 256×256 lattice at $t = 150$, $t = 200$, and $t = 1000$ after the quench at $t = 0$ ($\rho = 3.0$, $\kappa = 0.01$, $\tau = 0.6$). Because of the $\sqrt{3}/2$ scaling factor on the vertical direction, the shape of the real domain is rectangular. White regions correspond to the high density phase which is the minority phase at $\rho = 3.0$. One can clearly observe the different regimes: the early time spinodal decomposition at $t < 200$ and the late stage growth of homogeneous domains.

4 Time evolution of Minkowski functionals

We show in Figure 3 the typical time evolution of the local density across a 256×256 lattice after an off-symmetric quench ($\rho = 3.0$) from the initial temperature $T_{in} = 0.580$ to the final temperature $T_{fin} = 0.550$. At early times, one observes the decay of the unstable homogeneous phase as a result of the growth of density fluctuations. This spinodal decomposition regime is followed by the growth of homogenous droplets of the minority phase. Since the surface tension tends to reduce the interfacial energy, the high density phase evolves to a single domain having a circular shape (this final state is not shown in Fig. 3).

In contrast to Figure 3 we show in Figure 4 the typical time evolution of the local density across a 512×512 lattice after a nearly symmetric quench ($\rho = 3.45$). In this case, neither the high nor the low density domains dominate and, consequently, a bicontinuous pattern evolves. The morphology in Figure 4 is clearly different from the pattern shown in Figure 3, where isolated droplets of the minority phase occur. These qualitative features gained by visual inspection may be quantified using the Euler characteristic χ, which measures the connectivity of structures: χ vanishes in the last case, but has large positive values for the droplet structure. We expect the Minkowski functionals to be especially fruitful for the analysis of spinodal decomposition kinetics in three dimensions where the bicontinuous pattern is not restricted to a single density as

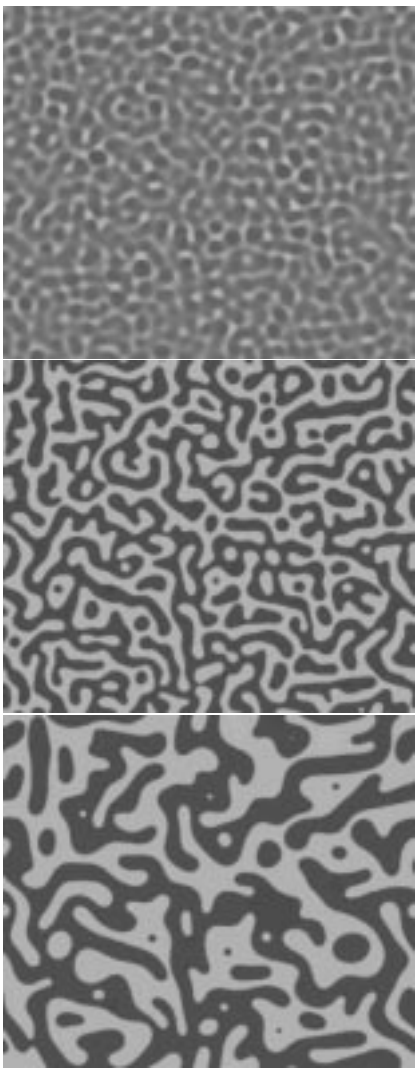

Fig. 4. Time evolution of the local density across a 512×512 lattice at $t = 200$, $t = 400$, and $t = 1000$ after the quench at $t = 0$ ($\rho = 3.45$, $\kappa = 0.01$, $\tau = 0.6$). White regions correspond to the high density phase. In contrast to Figure 3, the time evolution is nearly symmetric, *i.e.*, black and white domains evolve in an equal way leading to an interwoven bicontinuous pattern.

in the two-dimensional case but occurs in a large density region.

4.1 Dependence on threshold density ρ_{th}

First, we study the dependence of the morphological measures on the threshold density ρ_{th}. Figure 5 shows the corresponding Minkowski functionals calculated at the same moments as the snapshots in Figure 3. The early stage phase separation is evidentiated in Figure 5a by the displacement of the $F(\rho_{th})$ curve towards higher and respectively lower densities which corresponds to the formation of homogeneous domains with sharp boundaries. The two sharp kinks of $F(\rho_{th})$ are located at the coexisting mean

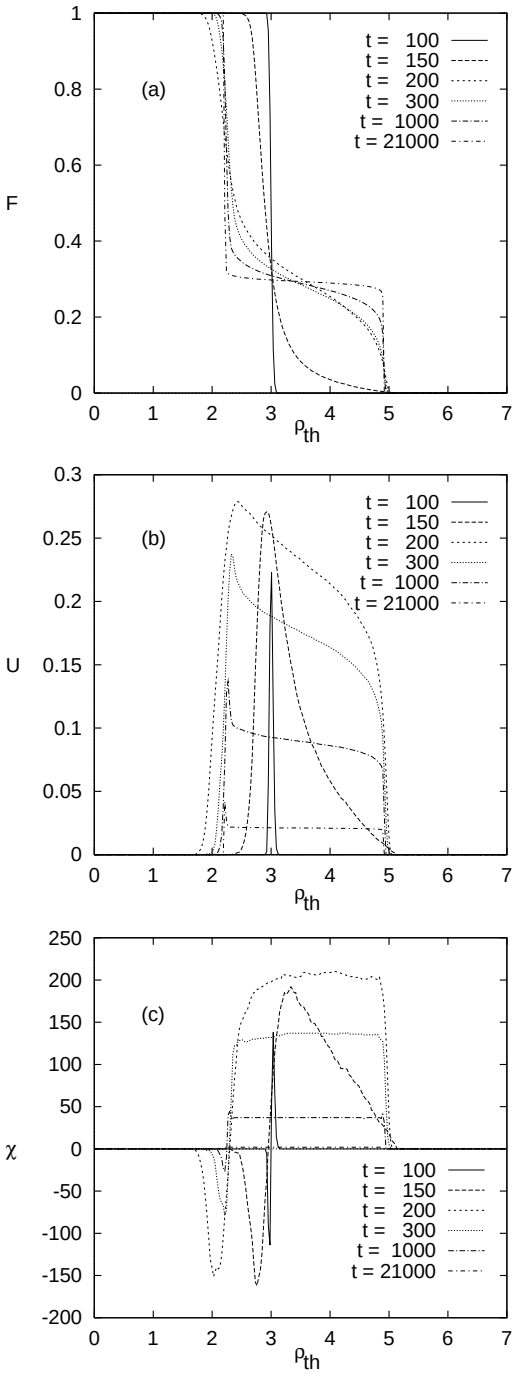

Fig. 5. Time evolution of the Minkowski measures depending on the threshold (computed at the same moments corresponding to the snapshots in Fig. 3). The two different regimes of the time evolution show up in the functional form of the measures. For early times one observes a strong threshold dependence of the measures due to the time evolution of the interfacial region between the homogeneous phases during spinodal decomposition. For late times the connectivity χ, for instance, is constant between the densities of the homogeneous phases indicating well-defined interfaces, whereas for early times $t < 200$ no such homogeneous domains exist. Because after $t \approx 200$ no significant threshold dependence occur in the measures, one can set the threshold to the medium density $\rho_{th} = 3.5$ in order to study the domain growth.

densities of the homogeneous domains at $T_{fin} = 0.550$, namely $\rho_{gas} = 2.236$ and $\rho_{liquid} = 4.839$, respectively. The functional form of $F(\rho_{th})$ is related to the interface profile between the homogeneous domains which sharpens during the spinodal decomposition. Additionally, the slope of $F(\rho_{th})$ in the central region decreases because the total volume of the interface region is reduced during this process, as a result of coalescence of high density domains. The slopes of $U(\rho_{th})$ and $\chi(\rho_{th})$ exhibit the same behavior in the central region, as one can see in Figures 5b and 5c.

Generally, one observes a crossover in the functional form of the measures, which is most clearly seen in the time evolution of the Euler characteristic $\chi(\rho_{th})$ shown in Figure 5c. For times $t < 200$, the dependence on the threshold is determined by the sharpening of interphase-boundaries, *i.e.* by the formation of homogeneous domains. The sharp peaks of negative connectivity in Figure 5c, for instance, is an artificial threshold phenomena due to noise in the initial density distribution because at a given threshold a lot of white pixels show up inside black domains before the whole region turns white. But after $t \approx 200$, the Euler characteristic becomes constant over a large interval determined by the coexisting densities, indicating that the connectivity does not depend on the threshold anymore, *i.e.*, that well-defined domains exist.

In Figure 6 we show the general appearance of the time evolution of the Minkowski functionals for three values of ρ_{th} at a typical mean density of the fluid ($\rho = 3.0$). A first general feature of these curves is that, for early times, *i.e.*, before $t \approx 200$, a strong dependence on ρ_{th} is observed due to the forming of sharp interfaces, as already mentioned when discussing the graphs in Figure 5.

For times $t > 200$ the differences become less and less pronounced. The still remaining differences in $F(t)$ are related to the density profile which interpolates smoothly between the coexisting densities. For a sharp kink profile no dependence on the threshold ρ_{th} would be registered. But changing the threshold yields changes of the area of white domains if the density profile is smooth, *i.e.*, one gets parallel borders situated at a distance $\epsilon(\rho_{th})$ depending on ρ_{th}. Using the relation (3.9) one obtains that the differences of the white area $F(t)$ (boundary length $U(t)$) is proportional to the boundary length $U(t)$ (Euler characteristic χ, respectively).

Because no significant threshold dependence of the Minkowski functionals is observed after $t \approx 200$, the threshold will be set further to the medium density value $\rho_{th} = 3.5$, when not mentioned otherwise.

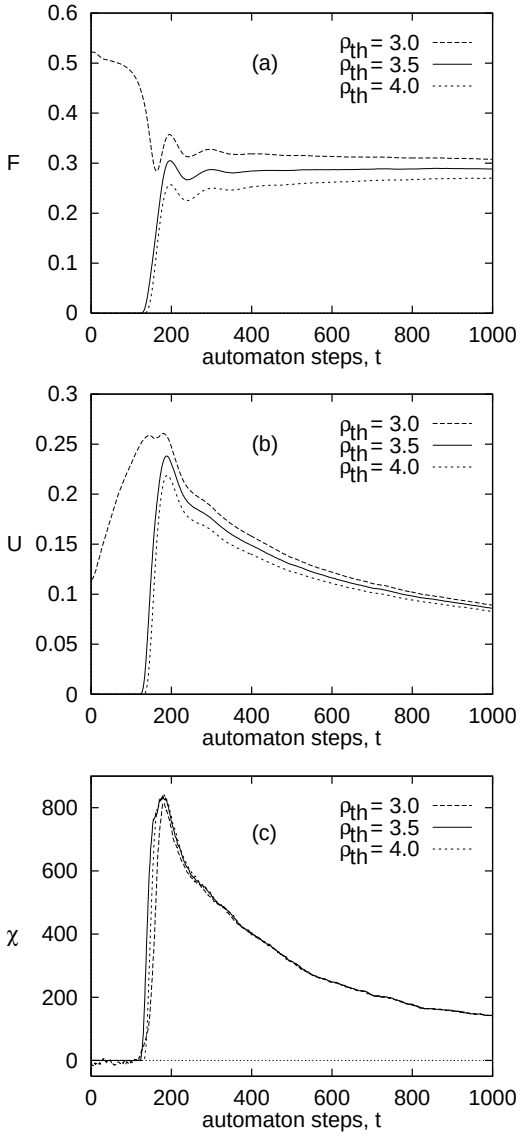

Fig. 6. Time evolution of the morphological measures F, U, and χ for three different thresholds, $\rho_{th} = 3.0,\ 3.5,\ 4.0$, at the mean density $\rho = 3.0$ and the parameters $\kappa = 0.01$, $\tau = 0.60$. After $t \approx 200$ no significant threshold dependence occur in the measures, the differences are proportional to the relative volume of the interfacial regions between high and low density domains, *i.e.*, to the boundary length U. One can distinguish two different time regime: an early stage spinodal decomposition with increasing measures (in particular, U and χ) and a late stage domain growth with decreasing boundary length U and Euler characteristic χ. The maximum values $\bar{U}$ and $\bar{\chi}$ define the transition time $\bar{t}$.

4.2 Crossover from spinodal decomposition to domain growth

In Figure 6 we have already shown the time dependence of the morphological measures $F(t)$, $U(t)$ and $\chi(t)$ for an off-symmetric quench ($\rho = 3.0$), where the fluid phase is the minority phase. In this figure, one can distinguish two different time regimes: the early stage of spinodal decomposition and the late state of domain growth. At early times, the growth of density fluctuations leads to the build up of interfaces between homogeneous domains of the two coexisting phases. This process is accompanied by an increase of white area F belonging to the liquid phase, as well as of the boundary length U of the interface. Also the Euler characteristic increases during this stage, because many disconnected components of the minority phase arise. In contrast to this early stage, the late stage domain growth is characterized by a decrease of the quantities U and χ,

which is a direct consequence of the increase of the characteristic length scale of the homogeneous domains.

The area of the liquid phase approaches the final value

$$F(t \to \infty) \to \frac{\rho - \rho_{gas}}{\rho_{liquid} - \rho_{gas}} \tag{4.1}$$

which is given by the level rule of the coexistence region shown in Figure 1. The oscillations of $F(t)$ in Figure 6a indicate shape fluctuations of the domains driven by the surface tension and the inertia of the fluid. These oscillations are intimately related to the formation of sharp interfaces which relax to their equilibrium value after the initial decomposition growth of the density fluctuations. Moreover, the oscillations are less favored at higher fluid viscosities established when using greater values of the relaxation time τ.

Because of the demixing of the phases, *i.e.* the growth of the domains, the boundary length U and the Euler characteristic approach their final minimum values

$$U(t \to \infty) \to 8\sqrt{\frac{F}{\pi N}}, \quad \chi(t \to \infty) \to 1 \tag{4.2}$$

which correspond to a single liquid drop with area F, immersed into the vapor phase. Their maximum values $\bar{U}$ and $\bar{\chi}$ mark the transition from the early stage increase to the late stage decrease, *i.e.* the crossover from the phase development during decomposition and the the successive domain growth. Consequently, their positions $t(\bar{U})$ and $t(\bar{\chi})$ may be used to define the transition (crossover) time $\bar{t}$ which marks the onset of domain growth and the end of the spinodal decomposition. Although the values of $t(\bar{U})$ and $t(\bar{\chi})$ generally differ slightly, the difference is quantitatively not relevant and both times mark the same transition in the time evolution. We will conventionally use the maximum of the boundary length U to define the transition time, *i.e.*, $\bar{t} := t(\bar{U})$. We note that it is difficult to determine the transition between these two obviously different dynamic regimes by analyzing, for instance, the time evolution of the correlation function instead of the time evolution of the morphology.

As a further example of possible applications of the morphological measures we discuss the dependence of the morphology on the surface tension κ. In Figure 7 we show the time evolution of the Minkowski functionals for three values of the surface tension κ when the relaxation time τ is kept constant. The amplitude of the oscillations of the white area F decreases when decreasing κ, *i.e.*, these oscillations are driven by surface tension which become important after the formation of the interfaces. The differences between the final values of F are related to the smooth density profile between the homogeneous phases determined by the surface tension. The interface region between the phases achieves a significant width for larger values of κ and, consequently, a decrease of the white area F is observed if the threshold is fixed. One can see that the growth process of the homogeneous domains at late times is also driven by the surface tension, *i.e.*, the decay process of $U(t)$ and $\chi(t)$ towards their final values

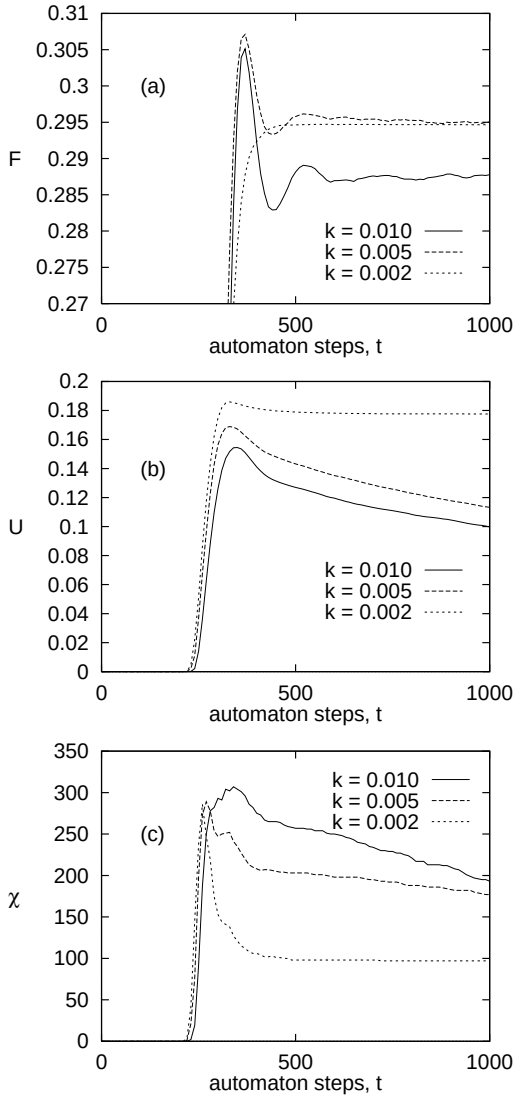

Fig. 7. Time evolution of the Minkowski measures for three different surface tensions $\kappa = 0.002,\ 0.005,\ 0.01$. ($\rho = 3.0$, $\tau = 0.8$, $\rho_{th} = 3.5$). The oscillations are driven by surface tension, *i.e.*, they vanish if κ is decreased.

becomes reduced when decreasing κ. On the contrary, the early time behavior is not affected significantly by the surface tension κ. In particular, the crossover time $\bar{t}$ from spinodal decomposition to domain growth has no significant dependence on κ. The maximum value of the boundary length $\bar{U}(\kappa)$ shown in Figure 7b decreases if κ is increased, because the domains become more spherical. This is the same reason, why the connectivity χ increases, because bridges between droplets break due to the decrease of boundary length. Thus κ has a relevant influence on the shape of the domains but does not influence significantly the characteristic length scale.

5 Scaling regimes

If the inhomogenous pattern consists of homogeneous domains with sharp interfaces, *i.e.*, if well-defined domains

exist, the domain growth process is achieved via the rearranging of domains without changing the relative area F of the liquid phase which is given by the level rule in equation (4.1). Because the measures $W_\nu(\mathcal{A})$ are homogenous functions of order $d-\nu$ (see Eq. (3.10)), we assume the following scaling behavior of the Minkowski functionals

$$F \sim 1, \quad U \sim L^{-1}, \quad \chi \sim L^{-2} \tag{5.1}$$

with the scaling length L. We have tested this assumption concerning the scaling behavior of the morphology by changing system parameters as surface tension κ and relaxation time τ, and looking for the same functional behavior of U^2 and χ.

There are other possibilities to define characteristic length scales of spatial patterns such as the first zero of the correlation function or the first moment of the wavelength distribution [3,4]. These definitions of the characteristic length, although widely used by many authors, are recognized to be computationally expensive [14]. The definition of the characteristic length L which is introduced using the scaling relation (5.1) allows a faster computation algorithm (it does not involve Fourier transformation, but only pixel counting) and has also a direct geometric interpretation. Additionally, we have the possibility to look for the scaling of the morphology given by the relations (5.1), *i.e.*, to test the scaling ansatz $U \sim L^{-1}$ and $\chi \sim L^{-2}$.

5.1 Early stage decomposition

The possibility to distinguish between the early time spinodal decomposition and the late stage domain growth, which are delimited by the transition time $\bar{t}$, enables to study the length scales and characteristic times at the very beginning of the phase separation. In particular, when approaching the spinodal density ρ_{sp}, the length $\bar{L}$ computed at the transition time $\bar{t}$ is expected to depend strongly on the viscosity τ and the density ρ. The length $\bar{L}$ can be defined starting either from the Euler characteristic $\bar{L}_\chi := \chi(\bar{t})^{-1/2}$ or from the boundary length $\bar{L}_U := U(\bar{t})^{-1}$. We expect the same functional dependence in both cases, except for a constant. The length scale $\bar{L}$ does not depend significantly on the surface tension κ as one can see in Figure 7 where the maximum value of the boundary length $\bar{U}(\kappa)$ and of the Euler characteristic χ is quite constant.

In order to test the scaling assumption (5.1) we study the dependence of $\bar{L}_\chi$ and $\bar{L}_U$ on the parameter τ, *i.e.* the viscosity. For fixed $\kappa = 0.01$ one observes that the position $\bar{t}$ of the maximum values is displaced towards larger times if τ is increased, *i.e.*, $\bar{t} \sim \tau$ and the relevant time variable is t/τ (see Fig. 8). For the same reason we observe that the frequency $\omega \sim \eta/\rho = \nu$ of the shape oscillations depends on τ and that the amplitudes of the oscillations are suppressed for large viscosities.

The maximum values $\bar{U}$ of $U(t)$, as well as $\bar{\chi}$ for the Euler characteristic decrease when increasing the viscosity. Thus, the characteristic length scale $\bar{L} = L(\bar{t}) \sim \bar{t}$ at the end of the decomposition regime (beginning of the domain growth) increases linearly with the transition time $\bar{t}$

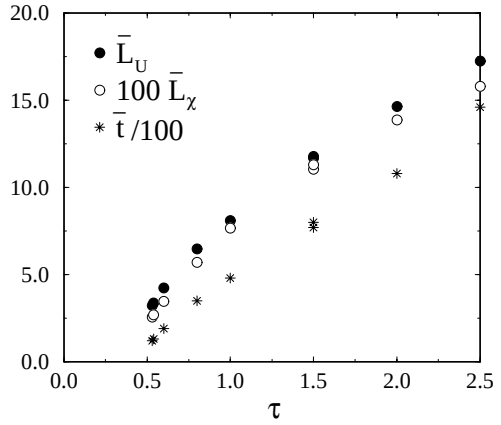

Fig. 8. Dependence of the characteristic length scales $\bar{L}_\chi := \chi(\bar{t})^{-1/2}$ (open circles) and $\bar{L}_U := U(\bar{t})^{-1}$ (filled circles), as well as of the onset of domain growth $\bar{t}$ (stars) on the viscosity τ ($\kappa = 0.01$).

indicating a density independent mean velocity $\bar{L}/\bar{t}$ of the fluid particles during the early stage. Moreover, one can see in Figure 8 that the length scales $\bar{L}_\chi \sim \bar{L}_U$ exhibit the same functional dependence on τ as predicted by the scaling assumption (5.1).

We address now the question how the morphological measures, *i.e.*, the Euler characteristic $\bar{\chi} := \chi(\bar{t})$ and the boundary length $\bar{U} := U(\bar{t})$ at the onset of domain growth depend on the mean density ρ. In Figure 9 we show some snapshots of the local density across a 256×256 lattice, which were taken at the crossover time $\bar{t}$ for fixed parameters $\kappa = 0.01$, $\tau = 0.8$, and $\rho_{th} = 3.5$, but for different mean densities ρ. One can clearly observe the dependence of the morphology at the onset $\bar{t}$ of domain growth *vs.* the mean density ρ, which is expressed by subsequent changes in the characteristic length scale $\bar{L}$, as well as in the connectivity measured by the Euler characteristic χ.

In Figure 10 we show $\bar{\chi}$ and $\bar{U}$ for different mean densities ρ at the same fixed parameters as the snapshots in Figure 9. First we note that we obtain a spinodal decomposition only in the density interval between the spinodal densities $\rho_{sp}^- = 2.744$ and $\rho_{sp}^+ = 4.315$ at $T = 0.55$ given by the instability condition $\psi''(\rho) \leq 0$. One observes a parabolic behavior for $\bar{U}(\rho)$ with a maximum for the bicontinuous patterns at the symmetric density $\rho = 3.5$. The Euler characteristic $\bar{\chi}(\rho)$ (mean curvature) is positive as long as the high density phase (white domains) is the minority phase forming many droplets within a sea of low density phase for $\rho < 3.5$. It becomes negative in the opposite case, according to equation (3.14), and zero for the symmetric decomposition indicating a vanishing mean curvature of the boundary lines.

It is interesting that, in the limiting case $\rho \to \rho_{sp}$, *i.e.*, when approaching the spinodal density $\rho_{sp}^- = 2.744$ at $T = 0.550$, we find the scaling behavior

$$\bar{L}(\rho) \sim (\rho - \rho_{sp}^-)^{-1/2} \tag{5.2}$$

for the characteristic length of the early stage spinodal decomposition (shown in Fig. 11). The spinodal density

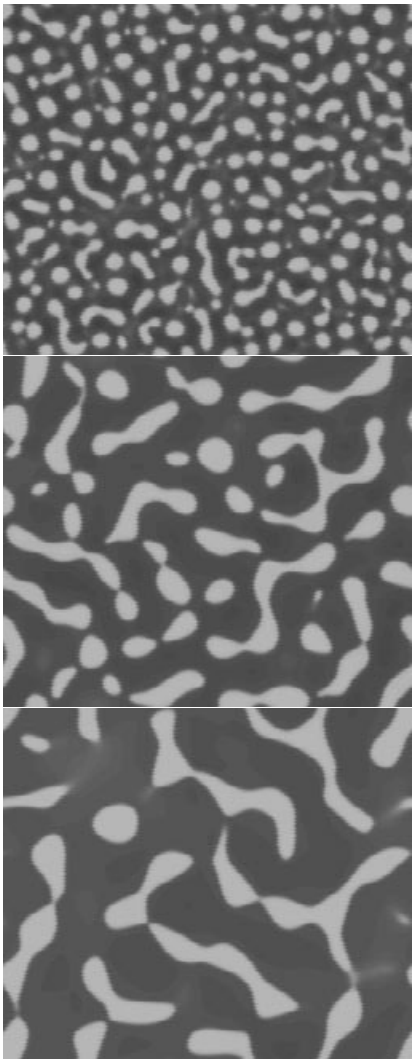

Fig. 9. Snapshot of the local density across a 256×256 lattice at the crossover time $\bar{t}$ for different mean densities (a) $\rho = 2.76$, $\bar{t} = 1140$; (b) $\rho = 3.0$, $\bar{t} = 330$; (c) $\rho = 3.5$, $\bar{t} = 280$. The parameters $\kappa = 0.01$, $\tau = 0.8$, $\rho_{th} = 3.5$ are held constant. The characteristic length scale $L(\bar{t})$ at the onset of the domain growth $\bar{t}$ increases when approaching the spinodal density $\rho_{sp}^{-} = 2.744$ whereas the connectivity decreases. The bicontinuous structures changes into a droplet phase which can be measured by the Euler characteristic χ shown in Figure 10.

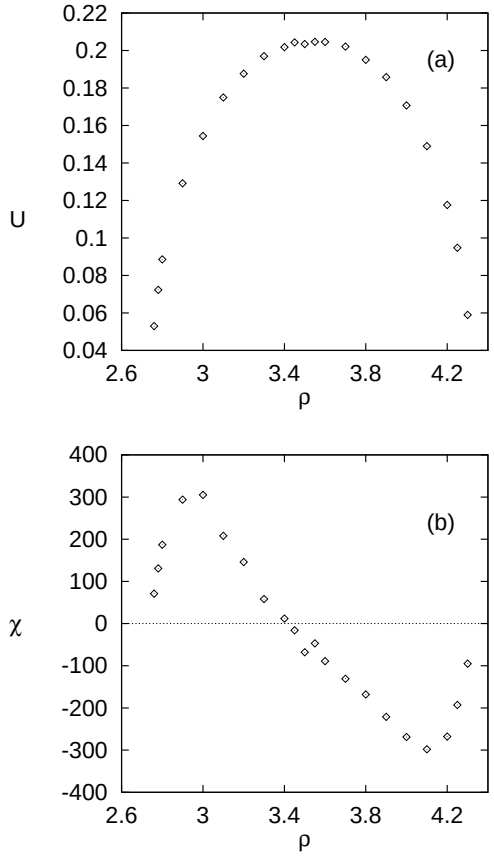

Fig. 10. Dependence of the Euler characteristic $\chi(\bar{t})$ and the boundary length $U(\bar{t})$ at the onset of domain growth on the mean density ρ (Same parameters as in Fig. 9). These measures describe the morphology of the patterns during spinodal decomposition at the mean density ρ. One observes a parabolic behavior for $U(\rho)$ with a maximum for the bicontinuous patterns at the symmetric density $\rho = 3.5$. The Euler characteristic (mean curvature) is positive as long as the high density phase (white domains) is the minority phase forming many droplets within a sea of low density phase for $\rho < 3.5$. It is negative according to equation (3.14) in the opposite case and zero for the symmetric decomposition indicating a vanishing mean curvature of the boundary lines.

ρ_{sp}^{-} found in the simulation is slightly below the predicted value given by the instability of the mean-field free energy (2.7). The scaling behavior (5.2) is consistent with the prediction of the Cahn-Hilliard theory for the growth of instable density modes [1]. For the onset time $\bar{t}$ we observe a similar behavior (see inset of Fig. 11)

$$\bar{t}(\rho) \sim (\rho - \rho_{sp}^{-})^{-1/2} \sim \bar{L}(\rho) \tag{5.3}$$

indicating a density independent mean velocity $\bar{L}/\bar{t}$ of the fluid particles during the early stage, which depends only on the temperature T. Cahn's linear theory of spinodal decomposition predicts for the time scale $\omega^{-1} \sim (\rho - \rho_{sp}^{-})^{-2}$ of the fastest growing mode when approaching the spinodal density, *i.e.*, a much faster increase than for $\bar{t}$.

5.2 Late stage domain growth

After the crossover time $\bar{t}$, the volume $F(t)$ has approached the final value given by equation (4.1). Despite the oscillations, we can consider this value as constant, because the domains are well-formed now. The time dependence of $F(t)$, *i.e.*, the relaxation to its final value is proportional to the boundary length $U(t)$ (see the dependence on the threshold ρ_{th}).

In Figure 12 we show the time dependence of $U^{-1}(t)$ and $\chi^{-1/2}(t)$, *i.e.*, the length $L(t)$ as function of time, in accordance with the relation (5.1). We observe the scaling

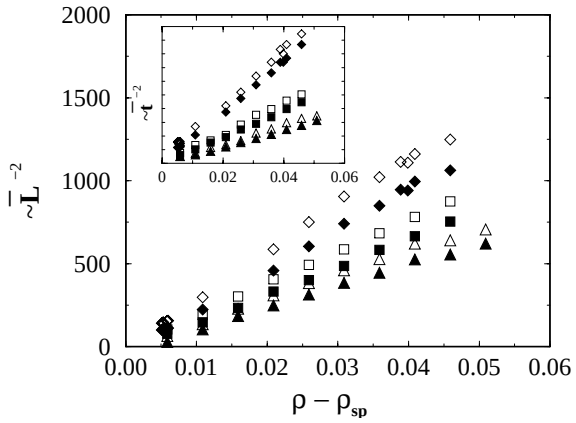

Fig. 11. Dependence of the characteristic length scale $\bar{L}(\rho) \sim (\rho - \rho_{sp}^{-})^{-1/2}$ at the onset of domain growth $\bar{t}$ on the mean density ρ for three different viscosities ($\tau = 0.6$ diamonds, $\tau = 0.7$, squares, $\tau = 0.8$ triangles). The length L can be measured by the Euler characteristic $\bar{L}_\chi := \chi(\bar{t})^{-1/2}$ (open symbols) or by the boundary length $\bar{L}_U := U(\bar{t})^{-1}$ (filled symbols). The inset shows the dependence of the time scale $\bar{t}$ of the spinodal decomposition on the mean density ρ. Again, the crossover time $\bar{t}(\rho) \sim \bar{L}(\rho)$ can be measured (arbitrary units) using the maximum of the Euler characteristic (open symbols) or the maximum of the boundary length (filled symbols), respectively.

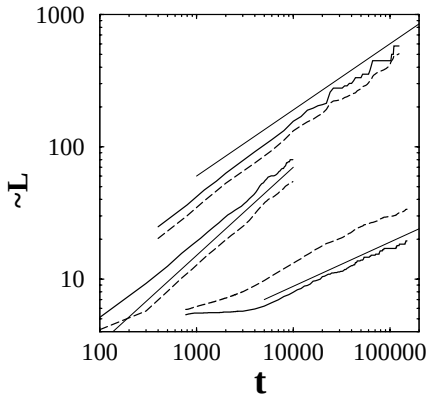

Fig. 12. Time evolution of the morphological measures $U(t)$ and $\chi(t)$ at different viscosities ($\rho = 3.0$, $\kappa = 0.01$, $\tau = 0.60$). The boundary length $w_1/U(t)$ (dashed line), and the connectivity $w_2/\chi(t)^{-1/2}$ (thick solid line) show the scaling relation (5.1) with the exponents $\alpha = 2/3$ ($\tau = 0.53$, $w_1 = 1$, $w_2 = 400$), $\alpha = 1/2$ ($\tau = 0.6$, $w_1 = 0.5$, $w_2 = 1000$), and $\alpha = 1/3$ ($\tau = 1.5$, $w_1 = 0.5$, $w_2 = 80$) indicated by thin solid lines. The coefficients w_i are chosen to separate the data.

behavior

$$L(t) \sim t^{\alpha} \tag{5.4}$$

with a scaling exponent α depending on the relaxation time τ (*i.e.*, the viscosity). We find three different scaling regimes, characterized by $\alpha = 2/3$ for low viscosities ($\tau = 0.54$), $\alpha = 1/2$ for intermediate values ($\tau = 0.8$), and $\alpha = 1/3$ for high viscosities ($\tau = 1.5$). The later one was not reported in reference [10], but is well-established by the Lifshitz-Slyuzov-Wagner theory [1]. For intermediate relaxation times τ we observe a crossover from one scaling exponent to the other, for example, from 2/3 (early times) to 1/2 (late times) at $\tau = 0.6$. At higher viscosities we do not observe scaling at all at least up to $t \sim 10^6$ time steps. For an off-symmetric quench the homogeneous domains are near-spherical droplets. We can define the mean curvature radius of these droplets by $R(t) := U(t)/\chi(t)$. This quantity shows scaling even for large domains at late times.

In contrast to reference [10] we interpret the scaling regime with $\alpha = 2/3$ not as the regime for long times although it is found for small viscosities. It is the same regime where we observe the strong oscillations in $F(t)$ and $U(t)$. As long as the fluid velocities are not damped by viscous forces the kinetic terms in the Navier-Stokes equation are dominant. This is the very early regime after spinodal decomposition and it can be seen only if the velocities are not damped by viscous forces. These velocities established at the beginning of the phase separation have little to do with the velocities established during domain growth, which are relevant for the exponent $\alpha = 2/3$ at very late times. The late stage accessible in our simulations is the regime with $\alpha = 1/2$ and $\alpha = 1/3$ which can be clearly seen in Figure 12.

We did several runs using the same parameters and obtained identical behavior. Therefore, the data we show in Figure 6 are obtained after individual runs without any averaging procedure, because such a procedure is not necessary in order to obtain accurate results. We emphasize that the statistical robustness of the morphological measures is essential for the determination of the length L, especially for small system sizes and for the late stage regime where statistical fluctuations become important. Generally, fluctuations of the measures are small due to the additivity relation (3.1) in contrast to the domain size calculated from the first zero of the radial distribution function. Therefore, one can extract reliable values for L from the morphological measures even in cases where this is not possible using the correlation function. The statistical robustness of the morphological measures is particularly demonstrated when determining the exponent $\alpha = 1/3$. As mentioned before, this exponent was not observed by other means using similar computer facilities.

We note that the calculation of U is less expensive than the calculation of the domain size $R(t)$, even when using Fast Fourier Techniques. For a 512×512 lattice, we need $\approx$ 1.5 minutes on the CM-5 machine to do 1000 lattice updates including the calculation of Minkowski measures, while for the calculation of $R(t)$ alone we need $\approx$ 8 minutes on the same lattice, despite the great effort made towards the optimization of the computing speed.

Finally, we mention that the time dependences of the Euler characteristic and the boundary length shown in Figure 12 are different in the beginning of the growth process. For instance, the slope for $\chi^{-1/2}(t)$ (solid line) at $\tau = 1.5$ ($\alpha = 1/3$) is much smaller than for $U^{-1}(t)$ (dashed line) at times $t < 5000$. This indicates a change of the morphology, *i.e.*, of the domain shape at early times. But the late stage scaling behavior is not affected by this initial rearrangement of the homogeneous phases. In

reference [35] the same morphological measures – which were already introduced in reference [5] – are used to study the morphology of spinodal decomposition in binary fluids. The observed' breakdown of scale invariance in the coarsening of phase-separating binary fluids' reported in reference [35] and, in particular, the statement that this happens at all times is related to the symmetry of the phases. Unfortunately, they do not report results for later times where a crossover to identical scaling behavior may occur. Also system parameters such as viscosity or surface tension are not given in reference [35] which are necessary to repeat or evaluate their data. The breakdown of scale invariance for a one-component fluid was already observed in reference [5] but only for early times.

6 Conclusions

The aim of this paper is to make an attempt towards the characterization of the time evolution of the morphology of phase separation, using morphological measures defined by the equations (3.1–3.3). For this purpose we use a lattice Boltzmann model on a 2D hexagonal lattice achieved in references [9–11] to model the isothermal hydrodynamics of a two phase system. A comparison of our results with simulations of Ginzburg-Landau models will be done in future work in order to elucidate, for instance, the differences between conserved and non-conserved order parameters.

Here, we focused on the general method and the advantages of using morphological measures to analyze inhomogeneous structures. Hadwiger's theorem (3.7) asserts that a morphological measure can be represented as a sum of $d+1$ Minkowski functionals which are familiar geometric quantities (in particular, for $d = 2$ these are the Euler characteristic χ, the covered area F, and the boundary length U).

In contrast to correlation functions, the Minkowski functionals are sensitive to changes in the shape and connectivity of the domains. We observe the scaling behavior (5.1) of the Minkowski functionals W_ν which makes it possible to define a *characteristic length scale* L of the domains. We obtain accurate values of the scaling exponent α for various hydrodynamic regimes (see Eq. (5.4)). In particular, we observe the $\alpha = 1/3$ behavior predicted by Lifshitz-Slyuzov-Wagner theory but not reported previously from the analysis of correlation functions of lattice Boltzmann simulations [9–11].

It is possible to observe the crossover from the early stage decomposition to the late stage domain growth and to obtain a clear definition of the early time regime of spinodal decomposition. We analyzed the morphology of patterns at early times and recovered the scaling behavior (5.2) for the decomposition regime when approaching the spinodal density predicted by the Cahn-Hilliard theory. Additionally, we obtained an immediate test of the *scaling assumption of the morphology* during spinodal decomposition and domain growth.

We want to emphasize that the calculation of the morphological measures is *convenient* and *fast* because one has to count only pixels. The definition and calculation of the characteristic length scale L by using the scaling of the morphological measures U and χ instead of the correlation function makes possible a considerable decrease in the computational effort of the simulation.

Even more important for the determination of the length L is the *statistical robustness* of the morphological measures due to the additivity relation (3.1), which allows reliable values for L from the morphological quantities even if the system size is small or in the late stage regime, where the number of homogeneous droplets vanish and statistical fluctuations become important.

There are two open questions which will be addressed in further work. First, we observe a possible scaling behavior with $\alpha = 1$ for high viscosities, but with different scaling behavior for U and χ during the early time regime. The different scaling seems to indicate a change in the shape of typical domains. Second, the morphological measures are a promising tool in three dimensions since the topology of the patterns changes even more drastically with the mean density ρ than in two dimensions. In particular, one finds a whole region of densities where the pattern is bicontinous. Since the late stage growth is expected to depend on the topology of the spatial structure, the morphological measures may provide means to study the dependence of the scaling behavior on the morphology.

The simulations were carried out on the CM-5 parallel machine at BUGH Wuppertal. V.S. is indebted to Professor Siegfried Dietrich for providing the possibility of a stay in his department and acknowledges also the financial support of the Romanian Ministry of Research and Technology, supervised through the Romanian Space Agency.

References

1. J.D. Gunton, M. Miguel, P.S. Sahni, in *Phase Transition and Critical Phenomena*, edited by C. Domb, J.L. Lebowitz, vol. 8 (Academic Press, New York, 1983).
2. A.J. Bray, Adv. Phys. **43**, 357 (1994).
3. H.E. Stanley, *Introduction to Phase Transitions and Critical Phenomena* (Clarendon Press, Oxford, 1971).
4. M.P. Allen, D.J. Tildesley, *Computer Simulation of Liquids* (Oxford University Press, Oxford, 1993).
5. K.R. Mecke, V. Sofonea, Phys. Rev. E **56**, R3761 (1997).
6. A. Rosenfeld, A.C. Kak, *Digital Picture Processing* (Academic Press, New York, 1976).
7. J. Serra, *Image Analysis and Mathematical Morphology*, Vols. 1, 2, (Academic Press, New York, 1982).
8. L.A. Santalò, *Integral Geometry and Geometric Probability* (Addison-Wesley, Reading, MA, 1976).
9. M.R. Swift, W.R. Osborn, J.M. Yeomans, Phys. Rev. Lett. **75**, 830 (1995).
10. W.R. Osborn, E. Orlandini, M.R. Swift, J.M. Yeomans, J.R. Banavar, Phys. Rev. Lett. **75**, 4031 (1995).

11. M.R. Swift, E. Orlandini, W.R. Osborn, J.M. Yeomans, Phys. Rev. E **54**, 5041 (1996).
12. H. Furukawa, Physica A **204**, 237 (1994)
13. P. Ossadnik, M.F. Gyure, H.E. Stanley, S.C. Glotzer, Phys. Rev. Lett. **72**, 2498 (1994).
14. E. Velasco, S. Toxvaerd, Phys. Rev. E **54**, 605 (1996).
15. O.T. Valls, J.E. Farrell, Phys. Rev. E **47**, R36 (1993).
16. T. Lookman, Y. Wu, F.J. Alexander, S. Chen, Phys. Rev. E **53**, 5513 (1996).
17. D.H. Rothman, Phys. Rev. Lett. **65**, 3305 (1990).
18. C. Appert, S. Zaleski, Phys. Rev. Lett. **64**, 1 (1990).
19. D.H. Rothman, S. Zaleski, Rev. Mod. Phys. **66**, 1417 (1994).
20. F.J. Alexander, S. Chen, D.W. Grunau, Phys. Rev. B **48**, 634 (1993).
21. S. Chen, T. Lookman, J. Stat. Phys. **81**, 223 (1995).
22. R.B. Rybka, M. Cieplak, D. Salin, Physica A **222**, 105 (1995).
23. U. Frisch, B. Hasslacher, Y. Pomeau, Phys. Rev. Lett. **56**, 1505 (1985).
24. D.H. Rothman, J.M. Keller, J. Stat. Phys. **52**, 1119 (1988).
25. S. Succi, R. Benzi, F. Higuera, Physica D **47**, 219 (1991).
26. S. Wolfram, J. Stat. Phys. **45**, 471 (1986).
27. R. Benzi, S. Succi, M. Vergassola, Phys. Reports **222**, 147 (1992).
28. S. Succi, G. Amati, R. Benzi, J. Stat. Phys. **81**, 5 (1995).
29. H. Hadwiger, *Vorlesungen über Inhalt, Oberfläche und Isoperimetrie* (Springer Verlag, Berlin, 1957).
30. K.R. Mecke, Ph.D thesis (in German), Ludwig-Maximilians Universität, München, (1993); *Reihe Physik*, Vol. 25 (Verlag Harri Deutsch, Frankfurt, 1994).
31. C. Likos, K.R. Mecke, H. Wagner, J. Chem. Phys. **102**, 9350 (1995).
32. K.R. Mecke, Th. Buchert, H. Wagner, Astron. Astrophys. **288**, 697 (1994).
33. K.R. Mecke, H. Wagner, J. Stat. Phys. **64**, 843 (1991).
34. K.R. Mecke, Phys. Rev. E **53**, 4794 (1996).
35. A.J. Wagner, J.M. Yeomans, Phys. Rev. Lett. **80**, 1429 (1998).